Accurate equilibrium structures of linear triatomic molecules from a combined theoretical–experimental method: The protonated nitrogen molecule, HN 2 +

Mirjana Mladenović, Marius Lewerenz

Version of Record: https://www.sciencedirect.com/science/article/pii/S0022285221001429
Manuscript_952bd9c025843f581ae834a7e7caa7c5

Accurate equilibrium structures of linear triatomic molecules from a combined theoretical-experimental method: The protonated nitrogen molecule, HN_2^+

Mirjana Mladenović[a,*], Marius Lewerenz[a]

[a] *MSME, Univ. Gustave Eiffel, CNRS UMR 8208, Univ. Paris Est Créteil, Marne-la-Vallée, F-77454, France*

Abstract

This article examines several strategies which can be used to derive molecular equilibrium structure from experimental data and extends our previously suggested method to HN_2^+. Full-dimensional rovibrational calculations are carried out for eight isotopologues of HN_2^+ using two *ab initio* potential energy representations. Rovibrational energies computed for rotational angular momenta J as high as 15 in both parities are used to derive theoretical vibration-rotation corrections to ground-state rotation constants B_0. These results are combined with the available experimentally derived B_0 values to determine the r_0, r_α, and r_e structures of the ion. Higher-order corrections beyond the vibration-rotation α constants are found to be essential for the structure determination. Our analysis is supported by graphical representations, illustrating the anticorrelation of the structural parameters. The r_0 structure is rationalized in terms of a structure projected onto the principal

*Corresponding author
Email addresses: mirjana.mladenovic@univ-eiffel.fr (Mirjana Mladenović), marius.lewerenz@univ-eiffel.fr (Marius Lewerenz)

a axis and examined for the isoelectronic series of linear triatomic molecules HCO^+, HCN, HN_2^+, HNC, and HOC^+.

Keywords:

HN_2^+, Equilibrium structure, r_0 structure, Rovibrational calculations, α constants, Theoretical spectroscopy

---

1. Introduction

Determination of the equilibrium structure of molecules is considered as one of the most basic goals of spectroscopy. Geometric parameters can be unambiguously deduced only from equilibrium rotational constants B_e, which are unfortunately not directly accessible experimentally. Theoretical models have to be used to account for the effect of the vibration-rotation coupling and to provide corrections to the effective rotational constants B_v for a vibrational state v, with a special interest in the zero-point correction, $\Delta B_0 = B_e - B_0$. **Except for diatomics and nonlinear triatomics the conversion of equilibrium rotational constants into an equilibrium structure requires informations on more than one isotopologue. The standard procedure assumes a common mass-independent structure, which is equivalent to the Born-Oppenheimer picture.**

The concept of the equilibrium structure is theoretically well founded within the Born-Oppenheimer approximation, that is, a molecule is described by a mass-independent potential energy surface (PES), so that the minimum of the PES uniquely defines the equilibrium structure of the molecule. Numerically exact quantum-mechanical calculations are then needed to establish a direct link

between a given PES and spectroscopic observables. Such an approach employs the exact rovibrational kinetic energy operator (no dynamical approximation) and the full PES (no re-expansion) in combination with numerically convenient methods, yielding a complete answer about molecular rovibrational dynamics associated with the applied PES. A common representation connecting experimental approaches and theory can be obtained by fitting the computed rovibrational energies to appropriate spectroscopic Hamiltonians.

We have recently developed a two-step procedure for deriving molecular equilibrium structures from numerically exact rovibrational energies [1, 2]. This approach was applied to determine spectroscopic parameters for isotopic variants (isotopologues) of the formyl cation, HCO^+, and the isoformyl cation, HOC^+, in excellent agreement with available experimental results [1]. The aim of the present work is to provide a similar spectroscopic characterization of the protonated nitrogen molecule, HN_2^+, also known as diazenylium. This is a linear molecular ion, characterized by a degenerate bending ν_2 vibration, a symmetric stretching ν_1 vibration, and an antisymmetric stretching ν_3 vibration.

In the present paper, we use two three-dimensional potential energy surfaces, developed for HN_2^+ in its ground electronic state, $\widetilde{X}^1\,\Sigma^+$, by *ab initio* computation. The first is the CCSD(T)/cc-pVQZ PES of Schmatz [3, 4], hereafter called SM PES. This is a global potential energy representation with two equivalent colinear minima, separated by an isomerization barrier $17\,137\,\mathrm{cm}^{-1}$ above the energy minima at the linear geometries. Low-lying

states of HN_2^+ are localized in one of the two wells. The double-well and nuclear spin symmetries are lifted for mixed nitrogen isotope forms. These issues are relevant when studying, for instance, interstellar isotope fractionation [5].

As the second PES, we use the ACTQ5+rel+ACPF quartic internal coordinate force field (QFF) of Huang, Valeev, and Lee [6], hereafter called HVL QFF. This PES includes one-particle basis set extrapolation, core-correlation, and scalar relativity, as well as higher-order correlation terms obtained by the averaged coupled-pair functional (ACPF) method. Huang *et al.* also reported corresponding vibrational frequencies and rotational parameters, computed by second-order vibrational perturbation theory. For our rovibrational variational calculations, HVL QFF was first transformed to Morse-cosine coordinates, as recommended previously [6, 7].

Quantum mechanical calculations of rovibrational energies for the protonated nitrogen molecules are performed combining a discrete variable representation for the angular motion with distributed Gaussian basis functions for the radial coordinates [8, 9]. Atomic masses are applied, as commonly done in similar studies. The computed rovibrational energies are used to extract the parameters of appropriate spectroscopic Hamiltonians in a least-squares analysis and to determine theoretical vibration-rotation corrections to the zero-point rotational constant B_0 (Section 2). The results for HN_2^+ and DN_2^+ are first employed to derive the stucture of the ion (Section 3) and to analyse the correlation between structural parameters (Section 4). The scope of the study is then broadened to include eight experimentally observed isotopologues (Section 5). **To analyze the notion of the r_0 struc-**

ture, obtained directly from the B_0 values, a comparative study of the isoelectronic series of linear triatomic molecules HCO^+, HCN, HN_2^+, HNC, and HOC^+ is carried out, revealing that the r_0 structure can be related to a structure projected onto the principal a axis (Section 6). Our theoretical procedure produces a highly consistent set of data, obtained within the Born-Oppenheimer approximation. Limitations arising from this approximation are also reviewed (Section 7).

2. Corrections to zero-point rotational constants

Following common practice of experiment, the rovibrational energies computed for a vibrational Σ state v are fitted to a standard spectroscopic power series expansion,

$$E_v(J) = T_v + B_v J(J+1) - D_v\, J^2(J+1)^2 + \cdots\,, \tag{1}$$

where T_v is the vibrational term energy, B_v the effective rotational constant, D_v the quartic centrifugal distortion constant, and so on, in a vibrational state v. For a vibrational Π state, we use

$$\begin{aligned} E_v(J) \;=\; & T_v + B_v \left[J(J+1) - \ell^2\right] \\ & - D_v \left[J(J+1) - \ell^2\right]^2 + \cdots \\ & \pm \tfrac{1}{2} \left[\, q_v J(J+1) + q_v^J\, J^2(J+1)^2 + \cdots \right]\,, \end{aligned} \tag{2}$$

where the rotational dependence of the ℓ-type doubling contribution is expressed in terms of $J(J+1)$, using the constants q_v, q_v^J, and so on.

We define the ground state vibrational correction ΔB_0 to the equilibrium rotational constant B_e as

$$\Delta B_0 = B_e^{\rm th} - B_0^{\rm th}\,, \tag{3}$$

where B_e^{th} and B_0^{th} are theoretical values of the rotational constant at equilibrium and in the ground vibrational state, respectively. In keeping with the notation previously used [1, 2], the spectroscopic correction S_0 to B_e is computed as

$$S_0 = \tfrac{1}{2}\,(\alpha_1 + \alpha_3) + \alpha_2\,, \quad \text{where} \quad \alpha_i = B_0 - B_i\,, \tag{4}$$

with α_i denoting the vibration-rotation interaction constant for the ith vibrational mode. Replacing B_0 and B_i with their theoretical values, we obtain the theoretical estimate S_0^{th}. The spectroscopic correction S_0 is accessible experimentally when the rotational constants for the ground state and the three fundamental vibrations are all known.

In the present work, rovibrational calculations for HN_2^+ and DN_2^+ are carried out for total rotational angular momenta as high as $J = 15$ for both SM PES and HVL QFF. The rovibrational energies are fitted using the third-order, fourth-order, and fifth-order spectroscopic Hamiltonians of Eqs. (1) and (2), producing three sets of parameters called Fit 3, Fit 4, and Fit 5, respectively. The fitted rotational energies go up to approximately $370\,\text{cm}^{-1}$ (11 THz). The fit standard deviations are better than 50 kHz for Fit 3, 40 Hz for Fit 4, and 5 Hz for Fit 5. A linear unweighted least-squares method [10] is applied to obtain Fit 3-Fit 5, implicitly assuming that the computed rovibrational energies form consistent sets of data of uniform quality. This assumption is reasonable for the modelling of the rotational transitions within a single vibrational state.

The potential energy minima of SM PES and HVL QFF are collected in Table 1, along with the associated equilibrium rotational constants B_e. The equilibrium bond distances r_e for SM PES are approximately 0.003 Å

Table 1: Potential energy minima $r_e^{\rm th}$ (in Å), associated rotational constants $B_e^{\rm th}$ (in MHz), and vibrational-rotation corrections ΔB_0 and $S_0^{\rm th}$ (both in MHz) obtained for the two potential energy representations.[a]

Parameter	SM PES	HVL QFF
$r_e^{\rm th}$(HN)	1.034 02	1.033 28
$r_e^{\rm th}$(NN)	1.095 62	1.092 78
$B_e^{\rm th}(HN_2^+)$	46 627.52	46 844.35
$B_e^{\rm th}(DN_2^+)$	38 560.87	38 727.41
Fit 3		
$\Delta B_0(HN_2^+)$	240.150 5(2)	240.550 5(2)
$\Delta B_0(DN_2^+)$	160.658 8(2)	160.648 7(2)
$S_0^{\rm th}(HN_2^+)$	245.748 1(11)	244.370 4(11)
$S_0^{\rm th}(DN_2^+)$	153.498 9(11)	151.743 7(12)
Fit 4		
$\Delta B_0(HN_2^+)$	240.148 807 97(29)	240.548 864 05(31)
$\Delta B_0(DN_2^+)$	160.657 278 90(33)	160.647 195 45(36)
$S_0^{\rm th}(HN_2^+)$	245.746 513 70(159)	244.368 722 13(174)
$S_0^{\rm th}(DN_2^+)$	153.496 193 94(240)	151.740 733 12(325)
Fit 5		
$\Delta B_0(HN_2^+)$	240.148 806 33(5)	240.548 862 29(4)
$\Delta B_0(DN_2^+)$	160.657 277 07(1)	160.647 193 41(2)
$S_0^{\rm th}(HN_2^+)$	245.746 511 51(20)	244.368 722 57(17)
$S_0^{\rm th}(DN_2^+)$	153.496 193 55(12)	151.740 738 02(18)

[a] Values in parentheses show one standard error to the last significant digit from the least-squares procedure.

longer than those for HVL QFF. Accordingly, B_e for SM PES is approximately 200 MHz smaller than B_e for HVL QFF. This trend is expected, given the different electronic structure methods used to construct the two potential energy representations.

Table 1 also provides the theoretical vibration-rotation corrections ΔB_0 and $S_0^{\rm th}$ to the ground vibrational state. Standard deviations of ΔB_0 and $S_0^{\rm th}$ are derived from the errors on the fitted spectroscopic parameters B_0, B_1, B_2, and B_3, which are in order of 10^{-4} MHz for Fit 3 to 10^{-8} MHz for Fit 5. Comparison of the values for ΔB_0 and $S_0^{\rm th}$ from Fit 4 and Fit 5 shows that the physical uncertainties related to the choice of the fitting model (number of centrifugal distortion constants) are at most $5{\cdot}10^{-6}$ MHz. This indicates an extremely high internal consistency in the set of computed rovibrational energy levels but is unrelated to differences with respect to experiment.

In Table 1, the values of ΔB_0 obtained for the two potential energy surfaces agree within 0.4 MHz and the values of $S_0^{\rm th}$ within 1.8 MHz. For a given PES, the difference between ΔB_0 and $S_0^{\rm th}$ is smaller than 10 Mz, ΔB_0 being smaller (larger) than $S_0^{\rm th}$ for HN_2^+ (DN_2^+). In our previous studies, we found that ΔB_0 and $S_0^{\rm th}$ differ by up to 50 MHz for the isotopic variants of HCO^+ and even 100 MHz for the isotopic variants of HOC^+ [1, 2].

From the experimental rotational constants $B_v^{\rm exp}$ reported by Yu *et al.* [11] for the ground vibrational state and three fundamental vibrations, the experimental vibration-rotation interaction constants $[\,\alpha_1^{\rm exp}, \alpha_2^{\rm exp}, \alpha_3^{\rm exp}\,]$ are determined to be [377.9, -104.5, 330.2] in MHz for HN_2^+ and [346.1, -136.0, 238.6] for DN_2^+. These values yield experimental spectroscopic corrections as $S_0^{\rm exp}(HN_2^+) =$ 249.6 MHz and $S_0^{\rm exp}(DN_2^+) = 156.1$ MHz. The theoretical results $S_0^{\rm th}$ in Ta-

ble 1 agree with the experimental counterparts within 5 MHz. Experimental uncertainties on $B_v^{\rm exp}$ are in the range up to 2 kHz.

Huang *et al.* [6] reported spectroscopic parameters obtained by the vibrational second-order perturbational approach, yielding the perturbational corrections $S_0^p(\mathrm{HN_2^+}) = 242.5\,\mathrm{MHz}$ and $S_0^p(\mathrm{DN_2^+}) = 161.3\,\mathrm{MHz}$. The value of $S_0^p(\mathrm{HN_2^+})$ agrees within 2 MHz with $S_0^{\rm th}(\mathrm{HN_2^+})$ of Table 1. On the other hand, $S_0^p(\mathrm{DN_2^+})$ differs from $S_0^{\rm th}(\mathrm{DN_2^+})$ by almost 10 MHz, being much closer to $\Delta B_0(\mathrm{DN_2^+})$ within 0.7 MHz instead. The perturbational vibration-rotation interaction constants $[\,\alpha_1^p, \alpha_2^p, \alpha_3^p\,]$ from [6] are explicitly $[\,373.8, \text{-}108.5, 328.3\,]$ in MHz for $\mathrm{HN_2^+}$ and $[\,369.9, \text{-}138.8, 230.2\,]$ for $\mathrm{DN_2^+}$. Our calculations for HVL PES give $[\,379.6, \text{-}110.3, 329.8\,]$ for $\mathrm{HN_2^+}$ and $[\,344.3, \text{-}139.7, 238.6\,]$ for $\mathrm{DN_2^+}$. Letting $\Delta_i = \alpha_i^p - \alpha_i^{\rm th}$, the differences $\{\Delta_1, \Delta_2, \Delta_3\}$ amount to $\{\text{-}5.8,\ 1.8,\ \text{-}1.5\}$ for $\mathrm{HN_2^+}$ and $\{\,25.6, 0.9, \text{-}8.4\,\}$ for $\mathrm{DN_2^+}$. It seems that the perturbational approach performs less well for $\mathrm{DN_2^+}$ and that the agreement of $S_0^p(\mathrm{DN_2^+})$ with $\Delta B_0(\mathrm{DN_2^+})$ is somewhat fortuitous in this case.

3. The equilibrium structure from the measurements on two isotopologues

The moment of inertia of a linear triatomic molecule ABC, with masses $m_{\rm A}$, $m_{\rm B}$, and $m_{\rm C}$ lying along the molecular axis, is

$$I = \frac{m_{\rm A}\, m_{\rm BC}}{M}\, d_1^2 + \frac{m_{\rm AB}\, m_{\rm C}}{M}\, d_2^2 + 2\,\frac{m_{\rm A}\, m_{\rm C}}{M}\, d_1\, d_2\,, \tag{5}$$

using $d_1 = r(\mathrm{AB})$ and $d_2 = r(\mathrm{BC})$. For the mass factors, we have $m_{\rm XY} = m_{\rm X} + m_{\rm Y}$ and $M = m_{\rm A} + m_{\rm BC}$. In terms of Jacobi coordinates r and R,

$$r = d_2 \quad \text{and} \quad R = d_1 + c_m\, d_2\,, \tag{6}$$

where $c_m = m_{\rm C}/m_{\rm BC}$, the moment of inertia I reads

$$I = \mu_r\, r^2 + \mu_{_R}\, R^2\,, \tag{7}$$

with $\mu_r = m_{\rm B}\, m_{\rm C}/m_{\rm BC}$ and $\mu_{_R} = m_{\rm A}\, m_{\rm BC}/M$.

Geometric arrangements of linear triatomic molecules are described by two bond distances. Spectroscopic measurements on at least two isotopic variants of a molecule are thus required for the determination of its equilibrium structure. We will first focus on triatomic molecules of the form AB_2, such as HN_2^+ and DN_2^+, for which $d_2 = r(\mathrm{NN})$ and $c_m = 1/2$. The rotational constants $B_e^{(1)}$ and $B_e^{(2)}$ for two isotopologues provide equilibrium moments of inertia $I_e^{(i)}$

$$I_e^{(i)} = \frac{\hbar^2}{2\, B_e^{(i)}} \tag{8}$$

for $i = 1$ and 2. The equilibrium distances follow as

$$\begin{aligned} r_e^2 =& F_m^{-1}\, \left[\mu_{_R}^{(2)}\, I_e^{(1)} - \mu_{_R}^{(1)}\, I_e^{(2)}\right], \\ R_e^2 =& F_m^{-1}\, \left[\mu_r^{(1)}\, I_e^{(2)} - \mu_r^{(2)}\, I_e^{(1)}\right], \end{aligned} \tag{9}$$

where

$$F_m = \mu_r^{(1)}\, \mu_{_R}^{(2)} - \mu_r^{(2)}\, \mu_{_R}^{(1)}\,, \tag{10}$$

implying

$$d_{2e} = r_e \quad \text{and} \quad d_{1e} = R_e - \tfrac{1}{2}\, r_e\,. \tag{11}$$

Uncertainties of the equilibrium distances can be estimated from the uncertainties of the equilibrium rotational constants by applying rules for error propagation. The corresponding results are summarized in Table 2, which

Table 2: Parameter uncertainties from the error propagation, with δ_q denoting the uncertainty of q and $\sigma^{(i)}$ the uncertainty of the equilibrium rotational constant $B_e^{(i)}$ of the ith isotopologue. The mass factor F_m is defined by Eq. (10).

Parameter	Uncertainty
$I_e^{(i)}$	$\delta_I^{(i)} = I_e^{(i)}\,[B_e^{(i)}]^{-1}\,\sigma^{(i)}$
r_e	$\delta_r = \frac{1}{2}\,r_e^{-1}\,F_m^{-1}\left[\mu_R^{(2)}\,\delta_I^{(1)} + \mu_R^{(1)}\,\delta_I^{(2)}\right]$
R_e	$\delta_R = \frac{1}{2}\,R_e^{-1}\,F_m^{-1}\left[\mu_r^{(2)}\,\delta_I^{(1)} + \mu_r^{(1)}\,\delta_I^{(2)}\right]$
d_{1e}	$\delta_{d1} = \delta_R + \frac{1}{2}\,\delta_r$

shows that the uncertainties of the structural parameters are linearly proportional to the uncertainties $\sigma^{(i)}$ of $B_e^{(i)}$. Rotational constants from microwave measurements are obtained regularly with much better accuracy than those from infrared measurements, so they are the preferred choice for the structure determination.

In the derivation of geometric parameters from experimentally determined $B_0^{\rm exp}$ values, three types of corrections to ground-state rotation constants are considered, leading to three different types of structure definitions. The use of $B_0^{\rm exp}$, uncorrected for vibrational effects, provides the so-called r_0 structure. Applying the spectroscopic correction S_0 to $B_0^{\rm exp}$, we generate a structure called the r_α structure. Finally, $B_0^{\rm exp} + \Delta B_0$ yields the r_e structure.

The geometric r_0, r_α, and r_e parameters derived using only data for HN_2^+ and DN_2^+ are summarized in Table 3. The millimeter wave spectroscopy values of Yu *et al.* [11] reported as $B_0^{\rm exp}(HN_2^+)$=46 586.875 29(49) MHz and $B_0^{\rm exp}(DN_2^+)$=38 554.749 38(93) MHz were combined with the vibration-rotation

corrections S_0 and ΔB_0 provided in Table 1. The structural parameters were then obtained using the analytical solutions of Eqs. (9)-(11).

The error limits in Table 3 are determined with the help of Table 2. The accuracy of the experimental $B_0^{\rm exp}$ values is in order of 10^{-4} MHz. As the accuracy of S_0 and ΔB_0 from Fit 5 in Table 1 is 10^{-7} MHz or better, the uncertainties of the structural parameters in Table 3 are primarily defined by σ_i of $B_0^{\rm exp}$. This is important so as not to spoil the information contained in $B_0^{\rm exp}$. We also note that Fit 4 provides values identical to those obtained using Fit 5. The results derived for Fit 3, which have approximately twice the uncertainty, are found to be statistically identical to the values shown in Table 3. The accuracy of the bond lengths is estimated to be much better than 10^{-6} Å in Table 3. This information should be viewed only as a measure of quality of the data sets and the procedure applied in the derivation according to the chosen mathematical model.

In Table 3, the values of r_α(HN) are longer than r_e(HN) by approximately 0.0015 Å, whereas r_α(NN) are shorter than r_e(NN) by approximately 0.0003 Å. The r_0 structure, computed from the uncorrected experimental $B_0^{\rm exp}$ values, differ from r_α and r_e by up to 0.004 Å. The results derived for SM PES and HVL QFF agree with each other within $9.5{\cdot}10^{-5}$ Å for the r_α structure and within $4{\cdot}10^{-5}$ Å for the r_e structure, differing thus beyond the stated error estimates. Bearing in mind that the two *ab initio* potential energy surfaces are of different nature, the agreement of the resulting structural parameters can be viewed as very satisfying.

The last two rows in Table 3 show experimental equilibrium structures. Owrutsky *et al.* [12] combined their infrared measurements with microwave

Table 3: Parameters (in Å) of the r_0, r_α, and r_e structures determined using the experimental ground state rotational constants reported for HN_2^+ and DN_2^+ by Yu *et al.* [11]. The theoretical corrections ΔB_0 and $S_0^{\rm th}$ obtained in Fit 5 of Table 1 are applied. The experimental equilibrium structures (Exp) reported by Owrutsky *et al.* (OGM) [12] and Amano *et al.* (AHT) [13] are additionally shown. Rotational constants are in MHz.[a]

	r(HN)	r(NN)	$B(HN_2^+)$
r_0	1.030 878 97(17)	1.096 748 74(4)	46 586.8753(5)
SM PES			
r_α	1.034 635 22(17)	1.092 689 15(4)	46 832.6218(5)
r_e	1.033 169 52(17)	1.093 033 35(4)	46 827.0241(5)
HVL QFF			
r_α	1.034 730 33(17)	1.092 690 63(4)	46 831.2440(5)
r_e	1.033 209 28(17)	1.093 020 62(4)	46 827.4242(5)
Exp			
OGM	1.033 59(43)	1.092 766(94)	46 840.40(110)
AHT	1.034 60(14)	1.092 698(26)	46 832.45(71)

[a] Values in parentheses show error limits obtained using Table 2.

and infrared data coming from different experimental groups, and fitted all spectral data in a global least-squares analysis to a general spectroscopic expansion of the form

$$\begin{aligned} G_{v,\ell,J} = & \sum_{i}^{3} \left(v_i + \tfrac{1}{2}\, d_i\right)\, \omega_i \\ & + \sum_{i,k\geq i}^{3} \left(v_i + \tfrac{1}{2}\, d_i\right) \left(v_k + \tfrac{1}{2}\, d_k\right) x_{ik} \\ & + \left(B_v \pm \tfrac{1}{2}\, q_v\right) \left[\, J(J+1) - \ell^2\right] \\ & - D_v \left[\, J(J+1) - \ell^2\right]^2 , \end{aligned} \tag{12}$$

where the effective rotational constant B_v for the vibrational state v is given by

$$\begin{aligned} B_v = & B_e - \sum_{i}^{3} \beta_i \left(v_i + \tfrac{1}{2}\, d_i\right) \\ & + \sum_{i,k}^{3} \gamma_{ik} \left(v_i + \tfrac{1}{2}\, d_i\right) \left(v_k + \tfrac{1}{2}\, d_k\right) . \end{aligned} \tag{13}$$

In the model of Eq. (12), the equilibrium rotational constant B_e appears as a fitting parameter. The constant β_i in Eq. (13) is sometimes called α_i and is close to, but actually not identical with the α_i constant defined in Eq. (4) as $\alpha_i = B_0 - B_i$. For the constant β_1, for instance, we have

$$\begin{aligned} \beta_1 &= B_0 - B_1 + 2\gamma_{11} + \gamma_{12} + \tfrac{1}{2}\gamma_{13} \\ &= \alpha_1 + 2\gamma_{11} + \gamma_{12} + \tfrac{1}{2}\gamma_{13} \, . \end{aligned} \tag{14}$$

Another set of experimental data in Table 3 is due to Amano *et al.* [13], who reported submillimeter-wave spectroscopy measurements on HN_2^+ and DN_2^+ in the ground state and for all fundamentals. To estimate higher-order

corrections to the ground-state rotation constants, Amano *et al.* [13] applied higher-order vibration-rotation coupling constants γ_{ij} available from other experimental studies on HN_2^+ and a similar system (HCN).

The experimental results in Table 3 differ from each other by up to 0.001 Å for the distances and by 8 MHz for B_e, i.e. considerably beyond the stated error limits. To investigate this situation, we compare in Table 4 the structural r_α parameters obtained using three sets of experimental data, which include in addition to B_0 also the values of B_1, B_2, and B_3 [11, 12, 13]. As seen there, the three experimental r_α structures are statistically identical, implying that the difference between the experimentally derived equilibrium bond distances r_e in Table 3 is solely due to the use of higher-order vibration-rotation contributions.

Table 4 also provides the parameters of the pure theoretical r_α structure, determined from the theoretical $B_0^{\rm th}$, $B_1^{\rm th}$, $B_2^{\rm th}$, and $B_3^{\rm th}$ values calculated for SM PES and HVL QFF. Comparing the r_α distances of Table 4 with the corresponding equilibrium r_e bond lengths shown in Table 1, we see that r_α(HN)-r_e(HN)=0.0015 Å and r_α(NN)-r_e(NN)=-0.0003 Å for both of the PESs. The r_α results do not reproduce the r_e values, implying that S_0 is not sufficient as a zero-point correction. **This finding is important for both experimental and theoretical spectroscopic studies. At the same time, the** rotational constant $B_\alpha = B_0 + S_0$ in Table 4 differs from the true B_e of Table 1 by only a few MHz (up to 6 MHz).

The higher-order vibration-rotation contribution C_0 to the ground-state rotational constant is defined here by

$$C_0 = B_\alpha - B_e\,, \quad \text{so that} \quad C_0 = S_0 - \Delta B_0\,. \tag{15}$$

Table 4: Structural r_α parameters (in Å) and associated rotational constants B_α (in MHz).[a] The experimental values are obtained using the spectroscopic data of Owrutsky *et al.* (OGM) [12], Amano *et al.* (AHT) [13], and Yu *et al.* (YPD) [11]. The theoretical values are derived for both SM PES and HVL QFF.

	r_α(HN)	r_α(NN)	$B_\alpha(HN_2^+)$
Experiment			
OGM	1.034 6(15)	1.092 6(3)	46 835.8(35)
AHT	1.034 632(3)	1.092 637 2(6)	46 836.462(7)
YPD	1.034 635(1)	1.092 636 7(2)	46 836.463(4)
Theory			
SM PES	1.035 50	1.095 27	46 633.12
HVL QFF	1.034 80	1.092 45	46 848.17

[a] Values in parentheses show error limits obtained using Table 2.

Table 5: Higher-order correction term C_0 (in MHz) effectively used by Owrutsky *et al.* (OGM) [12] and Amano *et al.* (AHT) [13], along with the theoretical counterparts calculated for both SM PES and HVL QFF.

	Experiment		Theory	
	OGM	AHT	SM PES	HVL QFF
$C_0(HN_2^+)$	-4.6	4.0	5.6	3.8
$C_0(DN_2^+)$	-12.3	2.7	-7.2	-8.9

The explicit values of C_0 are shown in Table 5. There, C_0 are up to about 12 MHz (0.000 4 cm^{-1}), so they are much smaller than S_0 of Table 1. Nevertheless, these higher-order correction terms C_0 have important consequences on the structural parameters, as easily visible in Table 3.

Whereas the theoretical C_0 corrections for HN_2^+ and DN_2^+ have different signs in Table 5, the experimental C_0 values for the two isotopic variants have the same sign. Since no sufficient information was available for DN_2^+, Amano *et al.* [13] estimated $C_0(DN_2^+)$ from the value $C_0(HN_2^+)$ by assuming its proportionality to the square of the rotational constant, so that $C_0(HN_2^+)$ and $C_0(DN_2^+)$ are both positive in Table 5. In the fitting procedure to Eq. (12), Owrutsky *et al.* [12] effectively included only one of the six higher-order coupling constants γ_{ij}, namely γ_{12}, which is reported to be $\gamma_{12}(HN_2^+)$= 9.31(17) MHz and $\gamma_{12}(DN_2^+)$= 24.60(78) MHz. In view of Eq. (13), we then have $C_0 = -\gamma_{12}/2$, so that $C_0(HN_2^+) = -4.6$ MHz and $C_0(DN_2^+) = -12.3$ MHz, as seen in Table 5.

4. Correlation between the structural parameters

Replacing I, d_1, and d_2 in Eq. (5) with their values at equilibrium, we easily find that

$$d_{1e} = -\frac{m_{\rm C}\, d_{2e}}{m_{\rm BC}} + \sqrt{\frac{M}{m_{\rm A}\, m_{\rm BC}} \left(I_e - \frac{m_{\rm B}\, m_{\rm C}}{m_{\rm BC}}\, d_{2e}^2 \right)} \tag{16}$$

or equivalently

$$d_{2e} = -\frac{m_{\rm A}\, d_{1e}}{m_{\rm AB}} + \sqrt{\frac{M}{m_{\rm AB}\, m_{\rm C}} \left(I_e - \frac{m_{\rm A}\, m_{\rm B}}{m_{\rm AB}}\, d_{1e}^2 \right)} \,. \tag{17}$$

Accordingly, a manifold of pairs (d_{1e}, d_{2e}) will reproduce the same I_e value, that is, the same equilibrium rotational constant B_e. The structural parameters d_{1e} and d_{2e} are anticorrelated by Eqs. (16) and (17), as a decrease of d_{1e} in (d_{1e}, d_{2e}) can be compensated by an increase of d_{2e} for a given B_e.

Figure 1 is a graphical representation of the pairs (d_{1e}, d_{2e}) which reproduce the experimental equilibrium rotational constants of Owrutsky *et al.* [12] and Amano *et al.* [13] for HN_2^+ and DN_2^+. The values of $B_e(HN_2^+)$ are listed in Table 3. The corresponding $B_e(DN_2^+)$ values are reported to be 38 722.9(25) and 38 708.38(58) MHz in [12] and [13], respectively. The case involving $B_e^{\rm exp}$ of Owrutsky *et al.* [12] is denoted with $X_{\rm Ow}$ and of Amano *et al.* [13] with $X_{\rm Am}$, using X=H and X=D for HN_2^+ and DN_2^+, respectively. The point of intersection of two lines is a structure (d_{1e}^c, d_{2e}^c) common to both isotopic forms, meaning that (d_{1e}^c, d_{2e}^c) simultaneously reproduces the rotational constants $B_e(HN_2^+)$ and $B_e(DN_2^+)$. The triangular points (▲) marked with Ow and Am in Fig. 1 are the experimental equilibrium distances reported by Owrutsky *et al.* [12] and Amano *et al.* [13], respectively, given

explicitly in Table 3. The equilibrium bond distances derived from the results of Owrutsky *et al.* [12] using the analytical solutions of Eqs. (9)-(11) are r_e^o(HN)=1.033 48(43) Å and r_e^o(NN)=1.092 793(93) Å. This pair is marked with $\mathrm{Ow_{corr}}$ (•) in Fig. 1. The two solutions, Ow and $\mathrm{Ow_{corr}}$, appear as different in Fig. 1. Taking into account their uncertainties, they are, strictly speaking, statistically compatible. **Given Fig. 1, we recommend to use our results $\mathbf{r_e^o}$(HN) and $\mathbf{r_e^o}$(NN) for future reference to the experimental equilibrium structure of Owrutsky *et al.* [12].**

The experimental r_e(NN) distances from [12] and [13] agree within the larger error bar of the earlier study, while the r_e(HN) distances are statistically incompatible. In order to quantitatively account for the intrinsic strong correlation between these structural parameters we used the stated error bars of the experimental B_e values and a Gaussian error distribution model and Eqs. (16) and (17) to construct the resulting probability densities $P(r_e(\mathrm{HN}), r_e(\mathrm{NN}))$ for the two experiments. The results are shown in Fig. 2. For an easier comparison both probability densities have been scaled such that their maximum value is equal to one. These most likely $r_e(\mathrm{HN}), r_e(\mathrm{NN})$ combinations correspond to the line intersections in Fig. 1 and are indicated by the solid innermost contours at $P = 0.99$. The other contours delimit the domains whose integrals correspond to 68.1% (dashed) and 95.3% (dotted) of the integral over the $r_e(\mathrm{HN}), r_e(\mathrm{NN})$ plane for the two experiments. These integrated probability values correspond to the 1σ and 2σ confidence intervals of a one-dimensional Gaussian. This two-dimensional analysis reveals that the two experimentally derived r_e structures are in fact incompatible for both parameters and that the projection on the r_e(NN) axis masks this

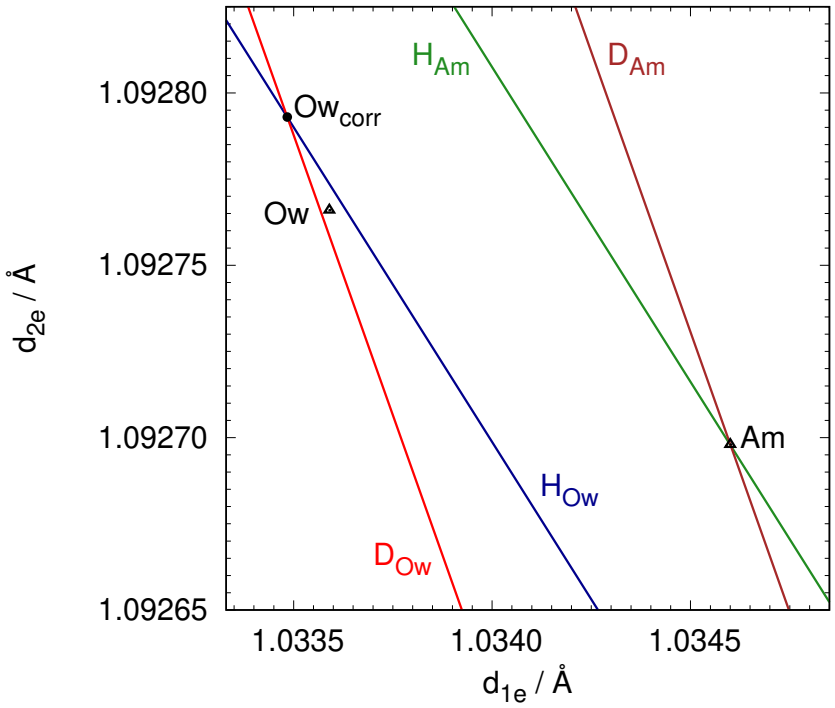

Figure 1: Pairs (d_{1e}, d_{2e}) reproducing experimental rotational constants of Owrutsky *et al.* [12] and Amano *et al.* [13] for HN_2^+ and DN_2^+, where $d_{1e} = r_e(\mathrm{HN})$ and $d_{2e} = r_e(\mathrm{NN})$. For more details, see Section 4 of the main text.

important fact.

5. The equilibrium structure from measurements on eight isotopologues

The rotational spectra of the protonated nitrogen molecule have been recorded at millimeter and sub-millimeter wavelengths for eight isotopologues involving ^{14}N, ^{15}N, H, and D [11, 14, 15]. Combining the values of B_0^{exp} from these studies with the theoretical vibration-rotation corrections from the present work, we produce three models B^{est} based on B_0^{exp}, $B_0^{\mathrm{exp}} + S_0^{\mathrm{th}}$,

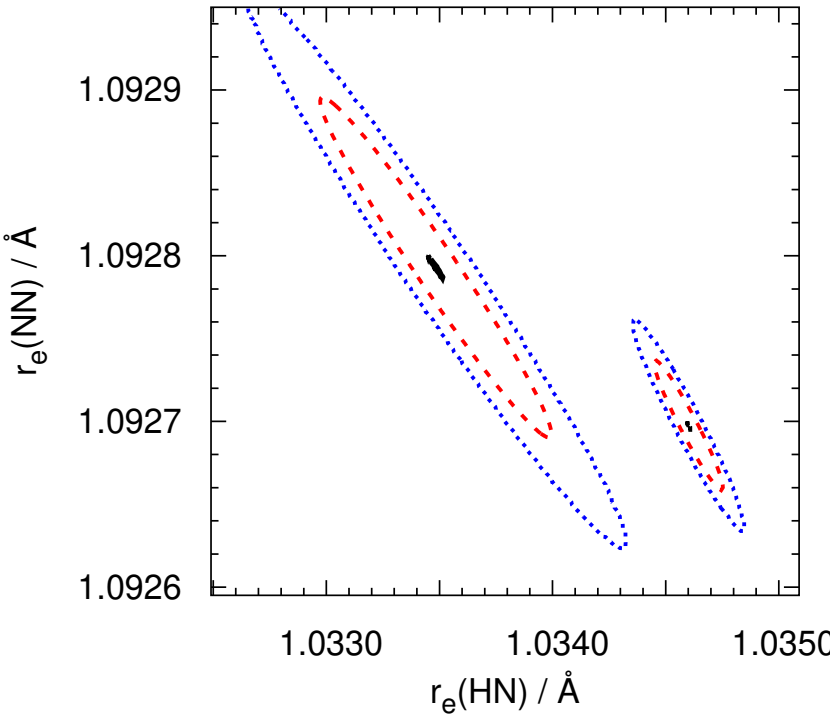

Figure 2: Probability densities $P(r_e(\mathrm{HN}), r_e(\mathrm{NN}))$ constructed from experimental B_e rotational constants and their uncertainties derived by Owrutsky *et al.* [12] (left) and Amano *et al.* [13] (right) for HN_2^+ and DN_2^+. Dashed and dotted contours enclose 68.1% and 95.3% of the total probability densities.

and $B_0^{\rm exp} + \Delta B_0^{\rm th}$, which are used to determine the r_0, r_α, and r_e structures, respectively, by means of a nonlinear least-squares technique (the Levenberg-Marquardt algorithm) [10].

The r_0, r_α, and r_e values computed from the data for eight isotopologues are summarized in Table 6. They are obtained in weighted least-squares fits. The laboratory results of Yu et at. [11] and Dore *et al.* [15] are employed, with experimental uncertainties varying from 0.000 13 MHz ($D^{15}N_2^+$) [15] to 0.000 93 MHz (DN_2^+) [11]. The uncertainties for the theoretical vibration-rotation corrections are taken from Table 1. To test the sensitivity of our results to these values, we also carried out unweighted nonlinear least-squares fits, denoted by Fit U in Table 6. The equilibrium distances found in the original and Fit U agree within $2{\cdot}10^{-6}$ Å. In Set C, the value for $B_0^{\rm exp}(HN_2^+)$ given as 46 586.875 29(49) MHz in [11] is replaced with the value of Cazzoli *et al.* [14] reported to be 46 586.875 49(18) MHz. **The resultant r_e values for Set C agree within $8{\cdot}10^{-6}$ Å with r_e from the original fits and are compatible with them within one standard deviation.** In Fit F_i, we employed r_e associated with one PES in combination with the corrections ΔB_0 from the other PES. In Fit F_2 for SM PES, for instance, r_e(NN) is kept constant at the value 1.093 017 Å associated with HVL QFF, yielding the bond distance r_e(HN)=1.033 219(5) Å, which agrees with r_e(HN)=1.033 209(9) Å for HVL QFF within one standard deviation. This increase of r_e(HN) resulting from the shortening of r_e(NN) is consistent with the fact that r_e(NN) and r_e(HN) are anticorrelated.

The equilibrium distances in Table 6 show spreads in the r_e(HN) and r_e(NN) values of $5{\cdot}10^{-5}$ Å and $2{\cdot}10^{-5}$ Å, respectively. The r_e(HN) values for

Table 6: Parameters of the r_0, r_α, and r_e structures (in Å) and the corresponding rotational constants B (in MHz), derived using the data for eight isotopologues of the protonated nitrogen molecule.[a]

Structure	r(HN)	r(NN)	$B(HN_2^+)$	rms[b]
r_0	1.030 86(21)	1.096 67(5)	46592.5(65)	2.93
SM PES				
r_α	1.035 01(16)	1.092 63(4)	46 831.9(52)	2.06
r_e	1.033 173(9)	1.093 029(2)	46 827.28(28)	0.13
r_e (Fit U)	1.033 172(10)	1.093 031(2)	46 827.20(32)	0.11
r_e (Set C)	1.033 166(11)	1.093 032(3)	46 827.21(34)	0.11
r_e (Fit F_1)	1.033 209	1.093 020(1)	46 827.44(8)	0.22
r_e (Fit F_2)	1.033 219(5)	1.093 017	46 827.56(8)	0.29
HVL QFF				
r_α	1.035 19(19)	1.092 62(5)	46 830.6(62)	2.43
r_e	1.033 209(9)	1.093 017(2)	46 827.70(28)	0.14
r_e (Fit U)	1.033 210(11)	1.093 018(3)	46 827.61(34)	0.13
r_e (Set C)	1.033 201(12)	1.093 019(3)	46 827.62(36)	0.12
r_e (Fit F_1)	1.033 173	1.093 026(1)	46 827.42(8)	0.20
r_e (Fit F_2)	1.033 163(5)	1.093 029	46 827.43(7)	0.23

[a] Values shown in parentheses are one standard deviation to the last significant digit from the least-squares procedure. Distances shown without error limits are kept constant in the fit.

[b] Root-mean-square error (rms) of the residuals is in MHz.

the two PESs agree within $4{\cdot}10^{-5}$ Å and the r_e(NN) values within $1{\cdot}10^{-5}$ Å. The estimates for r_e(HN) and r_e(NN) reproduce the fitted $B^{\rm est} = B_0^{\rm exp} + \Delta B_0$ values with root-mean-square (rms) deviations in order of 0.1 MHz.

The r_e results in Table 6, obtained in our combined theoretical-experimental approach, represent best estimates of the structural parameters. The $r_e^{\rm th}$ values for the high-quality *ab initio* HVL QFF surface deviate from these estimates by -$7\cdot10^{-5}$ Å for the HN bond length and by $24\cdot10^{-5}$ Å for the NN bond length. Our best estimate structures for HCO^+ and HOC^+ [1, 2] show comparable agreement with the *ab initio* structure determined by Koput [16] at the CCSD(T)/aug-cc-pV7Z level of theory with several high order corrections.

Table 6 is next compared with Table 3, which was derived by applying the rotational data for only two isotopologues. The equilibrium bond distances r_e(HN) and r_e(NN) from the two tables agree better than $4{\cdot}10^{-6}$ Å. The corresponding agreement for r_0(HN), r_0(NN), and r_α(NN) is within $8{\cdot}10^{-5}$ Å and for r_α(HN) within $5{\cdot}10^{-4}$ Å.

The three models for the rotational constant $B^{\rm est}$ are graphically compared in Fig. 3. Ranges of 0.004 Å along the abscissa and 0.001 Å along the ordinate are used in the two-dimensional graphs at the top and in the middle. The graph on the bottom covers a range of only 0.0005 Å along the abscissa and 0.0001 Å along the ordinate. The intersection of the horizontal and vertical dashed lines indicates the structural r_g parameters, that is, r_0 (top), r_α (middle), and r_e (bottom) from the all isotope least-squares fits. Their explicit values are listed in Table 6. Analogous to Fig. 1, a (red) line, representing one of the hydrogen-containing forms, and a (blue) line, representing

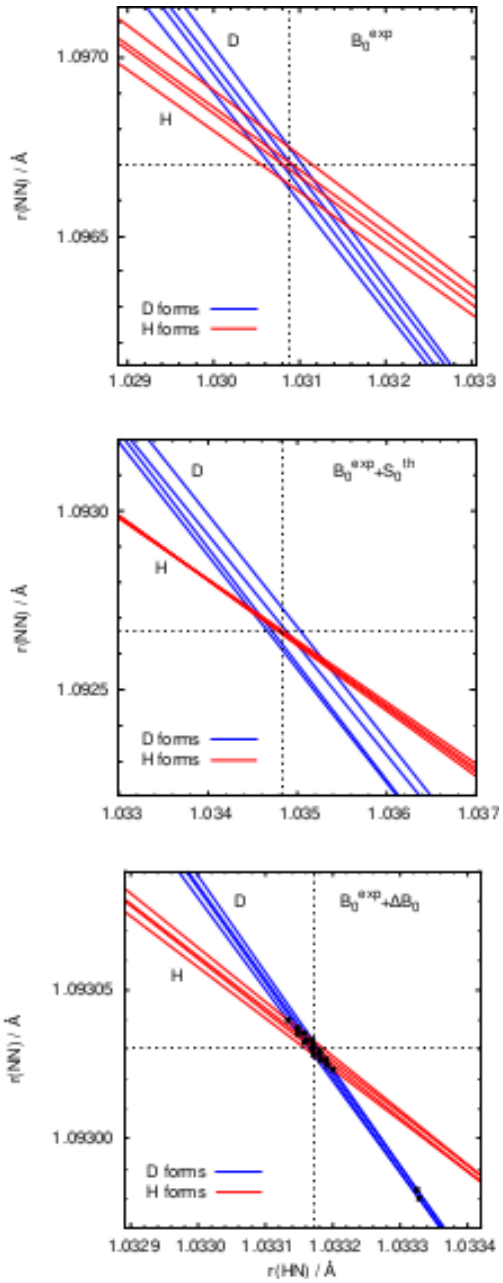

Figure 3: Pairs of the bond distances r(HN) and r(NN) reproducing $B^{\rm est}$ modeled as $B_0^{\rm exp}$ (top), $B_0^{\rm exp}+S_0^{\rm th}$ (middle), and $B_0^{\rm exp}+\Delta B_0^{\rm th}$ (bottom) for eight isotopologues of the protonated molecular nitrogen. Pair solutions for $B_0^{\rm exp}+\Delta B_0^{\rm th}$ (bottom) are shown by triangular points (▲).

one of the deuterium-containing forms, cross each other in the neighbourhood of r_g and define a compatible molecular geometry. The spreads of these crossing points around r_g become smaller when viewing Fig. 3 from the top to the bottom. Theoretical corrections computed for SM PES were applied in Fig. 3. Graphical representations of the results obtained using HVL QFF are identical to Fig. 3.

The Born-Oppenheimer approximation defines a mass independent common structure for all isotopologues. Consequently the correlation lines for all isotopologues should intersect in a single point. A residual spread could be indicative of non Born-Oppenheimer effects. It is clear that a search for such effects requires highly consistent equilibrium structure reconstructions and our proposed mixed experimental-theoretical method visibly shows the best internal consistency of the three strategies.

A pair determination of the molecular structure is frequently used in the literature. In the case when experimental data are known for n isotopic species, they can be paired in $n(n-1)/2$ different ways. From eight isotopic variants of HN_2^+, we thus have 28 possible pair solutions. These are shown for the case when $B^{\rm est} = B_0^{\rm exp} + \Delta B_0$ in Fig. 3 (bottom). Only 18 solutions are, however, visible over the range shown there. The mean values $r_{\rm ap}$ of all 28 pair solutions are 1.033 27 Å for $r_{\rm ap}$(HN) and 1.093 01 Å for $r_{\rm ap}$(NN), yielding $B_{\rm ap}(HN_2^+)$=46 827.5 MHz. Hence, $r_{\rm ap}$(HN) is 10^{-4} Å longer and $r_{\rm ap}$(NN) is $2{\cdot}10^{-5}$ Å shorter than their r_e counterparts in Table 6. The $r_{\rm ap}$ structure is sensitive to the choice of pairs or to the choice of parent species when **Kraitchman-Costain substitution** formulas [17, 18] are applied. In view of Fig. 3, we see that nonlinear least-squares methods appear more appro-

priate for the determination of molecular structures than the pair solution approach. This conclusion is in line with our previous finding for HCO^+ and HOC^+ [2].

^{15}N-substituted forms of HN_2^+ were first observed by Szanto *et al.* [19]. From the rotational $J = 0 - 1$ transition available for six isotopic forms at the time, these authors deduced a r_0 structure given by r_s(HN) = 1.032 00(10) Å and r_s(NN) = 1.094 70(40) Å. Using their rotational constants, we, however, find in an unweighted least-squares procedure that r_0(HN) = 1.030 90(40) Å and r_0(NN) = 1.096 70(8) Å. These improved r_0 values are in excellent agreement with the r_0 parameters shown in Table 6. Another r_0 estimate is due to Warner [20], who applied Kraitchman's relations for different parent species formed from a set of eight isotopologues. His pair solutions for eight parent species exhibit a large spread of $3{\cdot}10^{-4}$ Å, with a mean at r_{ap}(HN) = 1.030 41 Å and r_{ap}(NN) = 1.094 90 Å. Our least-squares solution derived from the data of Warner is r_0(HN) = 1.030 90(20) Å and r_0(NN) = 1.096 70(6) Å, in good agreement with the r_0 parameters of Table 6. **The r_0 values derived here from the experimental data of Szanto *et al.* [19] and of Warner [20] are recommended for future reference.**

6. The r_0 structure

To a first approximation, a molecule can be viewed as a set of oscillators, each of which executes vibrations about a well-defined equilibrium position r_e. The actual bond lengths in a vibrating molecule are then expected to be larger than the corresponding r_e values, that is, $r_0 > r_e$ for the ground vibrational state. This relation does not necessarily hold for linear molecules.

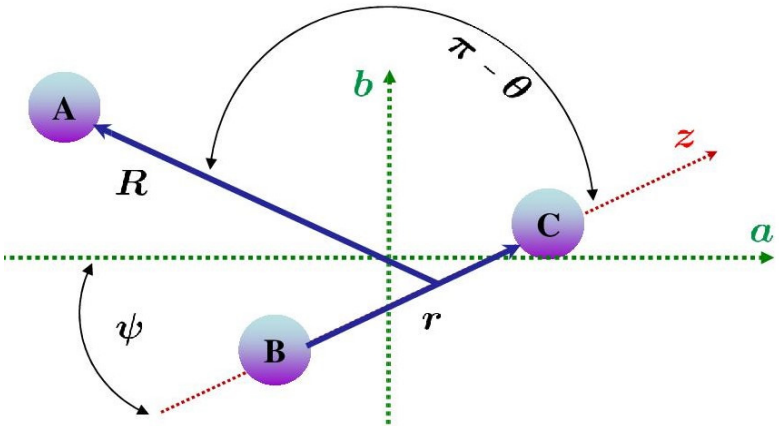

Figure 4: Jacobi coordinates (r, R, θ), the body-fixed z axis, the principal a and b axes, and the third Euler angle ψ for a triatomic molecule ABC.

We see, for instance, that $r_0(\mathrm{HN}) < r_e(\mathrm{HN})$ for HN_2^+ in Tables 3 and 6.

In the present rovibrational calculations, we have employed orthogonal (Jacobi) internal coordinates (r, R, θ) in the body-fixed formulation, where r is the NN bond length, R the distance from the proton to the center of mass of the N-N subunit, and θ the angle between the Jacobi vectors $\mathbf{r}$ and $\mathbf{R}$. The body-fixed z axis is aligned with the bond-distance vector $\mathbf{r}$ and the body-fixed $z \wedge x$ plane coincides with the molecular plane [21]. Our coordinates are schematically depicted in Fig. 4 for the case of a general triatomic molecule ABC.

The rotational contribution to the kinetic energy is strictly diagonal for the principal axis system. The direction perpendicular to the molecular plane is always a principal axis for triatomic molecules, that is, $c = y$. As seen in Fig. 4, the principal a and b axes are rotated in the molecular plane by an

angle ψ relative to the body-fixed z and x axes, where

$$\tan(2\psi) = -\frac{\mu_{_R}\, R^2\, \sin(2\theta)}{\mu_{_R}\, R^2\, \cos(2\theta) + \mu_r\, r^2}\,. \tag{18}$$

The angle ψ is the third Euler angle defining the instantaneous principal axis reference frame.

The vibrationally averaged structure of a linear molecule is nonlinear. This is seen in Table 7, where we compare the vibrationally averaged geometries in the ground vibrational state for the isoelectronic series of linear triatomic molecules HCO^+, HCN, HN_2^+, HNC, and HOC^+. Both hydrogen containing and deuterium containing isotopic forms are considered. In these calculations, SM PES is used for HN_2^+, a global three-dimensional CCSD(T)/cc-pVQZ PES for HCO^+/HOC^+ [9], and a CCSD(T)/aug-cc-pCVQZ PES for HCN/HNC [22]. The experimental r_0 parameters derived for HCN and HNC by Pearson *et al.* [23] are used in Table 7.

In addition to the expectation value $\langle\theta\rangle$ of the Jacobi angle, Table 7 also provides the expectation value of the Legendre polynomial $P_2 = (3\,\cos^2\theta - 1)/2$ and the expectation value of the Euler angle ψ. The amplitude of the bending motion varies between 7° for DCO^+ and 16° for HOC^+. This evolution is best demonstrated by Fig. 5, showing the minimum energy paths along the Jacobi angle. The stiffest profile there belongs to HCO^+ and the softest to HOC^+. The effective bending wavenumbers ΔE_2 in Table 7 are computed as $E(0,1^1,0;1,1) - E(0,0,0;1,1)$, with $E(v_1, v_2^\ell, v_3; J, p)$ denoting the energy of the vibrational state (v_1, v_2^ℓ, v_3) for rotational angular momentum J and parity p. The highest ΔE_2 value is associated with HCO^+ and the lowest with DOC^+.

In spectroscopic studies, the r_0 structure is derived directly from the

Table 7: Vibrationally averaged structural parameters $\langle\theta\rangle$, $\langle P_2\rangle$, $\langle\psi\rangle$, $\langle r_{\rm AB}\rangle$, $\widetilde{r}_{\rm AB}$, $\langle r_{\rm BC}\rangle$, and $\widetilde{r}_{\rm BC}$ in the ground vibrational state, zero-point energies E_0, and fundamental transitions $\Delta E_2, \nu_1$, and ν_3, as well as r_e and r_0 values for the isoelectronic series of linear triatomic molecules HCO^+, HCN, HN_2^+, HNC, and HOC^+. Distances are in Å, angles in degree, and energies in cm^{-1}. For detailed parameter definitions, see Section 6 of the main text.

Molecule	$\langle\theta\rangle$	$\langle P_2\rangle$	$\langle\psi\rangle$	$\langle r_{\rm AB}\rangle$	$\widetilde{r}_{\rm AB}$	$\langle r_{\rm BC}\rangle$	$\widetilde{r}_{\rm BC}$	E_0	ΔE_2	ν_1	ν_3	r_e(AB)	r_0(AB)	r_e(BC)	r_0(BC)
HCO^+	7.83	0.972	-2.26	1.114	1.097	1.113	1.112	3524.6	827.8	3086	2179	1.092[a]	1.091[a]	1.106[a]	1.109[a]
DCO^+	7.00	0.978	-2.03	1.108	1.095	1.113	1.112	2946.1	665.1	2580	1901				
HCN	8.59	0.967	-2.72	1.084	1.065	1.159	1.158	3476.3	712.0	3311	2100	1.066[b]	1.062[c]	1.154[b]	1.157[c]
DCN	7.66	0.974	-2.44	1.079	1.064	1.159	1.158	2884.9	568.7	2631	1928				
HN_2^+	9.19	0.962	2.95	1.054	1.035	1.101[d]	1.099	3507.8	686.8	3235	2257	1.033[e]	1.031[e]	1.093[e]	1.097[e]
DN_2^+	8.17	0.970	2.64	1.049	1.034	1.100[d]	1.099	2921.2	544.3	2636	2024				
HNC	168.58	0.942	4.19	1.013	0.986	1.176	1.173	3371.6	464.3	3657	2025	0.996[b]	0.986[c]	1.170[b]	1.173[c]
DNC	169.87	0.954	3.72	1.009	0.987	1.176	1.173	2769.3	363.7	2790	1939				
HOC^+	163.85	0.886	6.13	1.011	0.962	1.166	1.160	2871.1	242.1	3277	1901	0.990[a]	0.965[a]	1.154[a]	1.159[a]
DOC^+	165.23	0.904	5.62	1.005	0.964	1.166	1.160	2357.6	175.3	2483	1840				

[a] Parameters from [2].

[b] Minima for the CCSD(T)/aug-cc-pCVQZ PES [22].

[c] Experimental results from [23].

[d] Explicit values are $\langle r_{\rm HN}\rangle = 1.100\,6$ Å and $\langle r_{\rm DN}\rangle = 1.100\,4$ Å.

[e] Values from Table 6.

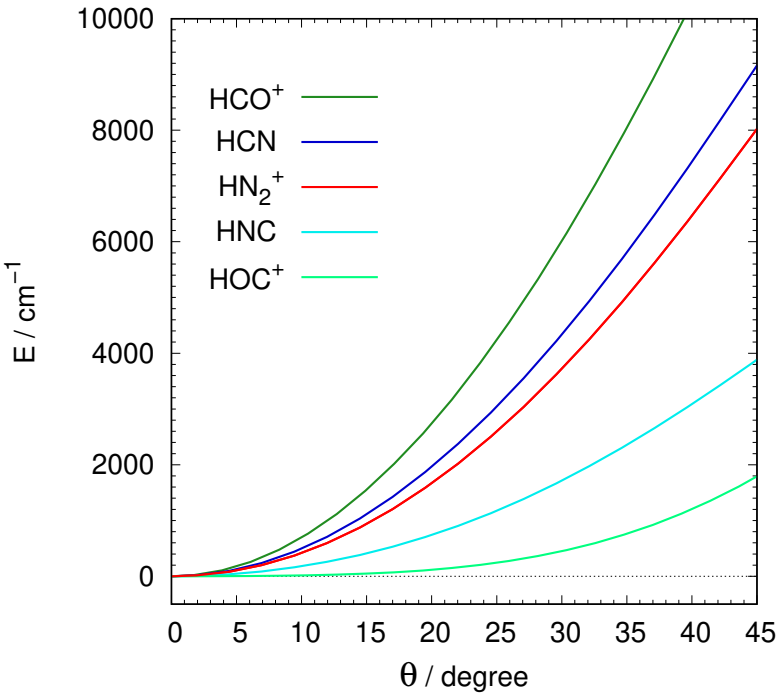

Figure 5: Minimum energy paths along the Jacobi angle θ measured relative to the energy of the respective optimum equilibrium configuration for the isoelectronic series of linear triatomic molecules HCO^+, HCN, HN_2^+, HNC, and HOC^+.

experimentally determined zero-point rotational constants B_0. For linear triatomic molecules this approximation effectively means that

$$I_0 = \mu_r r_0^2 + \mu_R R_0^2 \,, \tag{19}$$

where $I_0 = \hbar^2/2B_0$. The values of r_0 and R_0, computed using Eq. (19), differ from the expectation values $\langle r \rangle$ and $\langle R \rangle$ since the vibrationally averaged structure is nonlinear, as exemplified in Table 7. As a way of linearizing a real vibrating molecule, we introduce here a structure projected onto the principal a axis (the axis with least moment of inertia), for which we use

the parameters $\widetilde{r}_{\rm AB}$ and $\widetilde{r}_{\rm BC}$, with $\widetilde{r}_{\rm XY}$ denoting the projection of the bond-distance vector $\mathbf{r}_{\rm XY}$ onto the a axis. The $\widetilde{r}_{\rm AB}$ and $\widetilde{r}_{\rm BC}$ values in Table 7 are calculated from the expectation values $\langle r\rangle$, $\langle R\rangle$, $\langle\theta\rangle$, and $\langle\psi\rangle$ obtained in $J = 0$ calculations.

For the isoelectronic series of linear triatomic molecules, Table 7 reveals that $\langle r\rangle > r_e$ actually holds for the vibrationally averaged bond lengths for both $r_{\rm AB}$ and $r_{\rm BC}$. We also see that $r_0({\rm AB}) < r_e({\rm AB})$ and $r_0({\rm BC}) > r_e({\rm BC})$, where AB is the bond distance involving a light atom (H or D), placed farthest away from the a axis in Fig. 4. The values of $\langle r_{\rm AB}\rangle$ are longer than r_0(AB), with differences ranging from 0.017 Å for DCO^+ to 0.046 Å for HOC^+. At the same time, $\widetilde{r}_{\rm AB}$ and r_0(AB) are closer to each other, deviating by at most 0.006 Å. We also observe that $\langle r_{\rm HB}\rangle$ and $\langle r_{\rm DB}\rangle$ differ by 0.005-0.006 Å, whereas the difference between $\widetilde{r}_{\rm HB}$ and $\widetilde{r}_{\rm DB}$ is only 0.001-0.002 Å. The bond-distance vector $\mathbf{r}_{\rm BC}$ between heavy atoms is tilted by the Euler angle ψ relative to the a axis in Fig. 4. Since $\langle\psi\rangle = 2$ - 6°, $\langle r_{\rm BC}\rangle$ and $\widetilde{r}_{\rm BC}$ are similar, differing by at most 0.006 Å for HOC^+.

In view of Table 7, we may infer that $\widetilde{r}_{\rm AB}$ and $\widetilde{r}_{\rm BC}$ are good approximations for the structural r_0 parameters. This statement should, however, be viewed only as a qualitative rationalization since vibrationally averaged quantities are J-dependent [2]. This in itself is to be perceived as an inherent conceptual problem for the definition of the r_0 structure.

The difficulties in determining molecular structures from zero-point rotational constants B_0 are clearly visible in Fig. 3 (top): the intersection points of the correlation lines there show a large spread and a geometric structure common to different (actually all) iso-

topologues is impossible to find. In the mass-dependence (r_m) method proposed by Watson [24], the equilibrium moment of inertia is approximated with $2I_s - I_0$, where I_s is the moment of inertia computed for the substituted r_s geometry. This approach was, however, found unsatisfactory for hydrogen containing species [24].

7. Final remarks

Microwave rotational spectroscopy measures the energies of rotational transitions, frequently with stunning precision. The experimental observations are fitted to effective spectroscopic Hamiltonians following the linear-molecule or nonlinear-molecule formalism and the derived spectroscopic parameters are commonly applied to derive the molecular equilibrium structure. Yet this task is far from straightforward. In real vibrating-rotating molecules, corresponding to the actual experimental situation, the ground vibrational state is described by a wavefunction, extended over other-than-equilibrium arrangements. The effects of zero-point vibrational motion produce an effective rotational constant B_0, which is different from the equilibrium B_e value, which is essential for the determination of the molecular structure. The rotational constant B_0 is not an observable, but a parameter arising within the model used to describe the rotation. There is no obvious way to derive $\Delta B_0 = B_e - B_0$ experimentally.

In the present work, the methods commonly used to correct the experimental rotational constant B_0 for the vibration-rotation interaction effects are examined by theoretical means for the case of the protonated nitrogen molecule, HN_2^+. The concepts of B_0 and B_e are both well founded **in**

the Born-Oppenheimer picture, providing a clear definition for the full vibration-rotation correction to B_0, given simply by the difference $\Delta B_0 = B_e - B_0$. Different potential energy representations (may) support different minima, however. This issue is addressed here by employing two PESs for HN_2^+, a global PES based on the CCSD(T)/cc-pVQZ approch [3] and a quartic force field based on the ACTQ5+rel+ACPF approach [6]. Both PESs lead to very similar ΔB_0 estimates which therefore appears to be a rather robust and useful quantity. **It is reasonable to expect that similar conclusions will be drawn also for other potential energy representations [25] available for HN_2^+ in the literature.**

The rovibrational energies for eight isotopologues of HN_2^+ and two *ab initio* PESs are obtained in numerically exact full-dimensional rovibrational calculations for rotational angular momentum J as high as 15 in both parities. The computed energies are easily fitted to highly accurate low-order effective spectroscopic Hamiltonians. This can be viewed as a hint towards regular rovibrational behaviour, in agreement with conclusions from our wavefunction analysis.

The spectroscopic correction S_0 of approximately 200 MHz for eight isotopic variants of HN_2^+ is the dominant contribution to the full correction ΔB_0. The higher-order corrections $C_0 = S_0 - \Delta B_0$ amount to several MHz and are thus much smaller than S_0. Although small, the contribution C_0 is found to be essential for the determination of the molecular structure. This is exemplified by Fig. 3, which graphically represents the solution for the structural parameters common to eight isotopologues of HN_2^+ obtained using three different models for the estimates B^{est} of the equilibrium rotational

constants B_e. Visibly the highest degree of consistency for the molecular geometry is obtained by combining our variationally computed ΔB_0 values with accurate experimental data. It is also evident that the accuracy of the geometry determination is not limited by the experimental accuracy but by shortcomings in the theoretical model for the $B_0 \rightarrow B_e$ correction. The corrections derived on the basis of low order perturbational formulas clearly do not provide sufficient accuracy.

A similar representation for HCO^+ is presented in Fig. 6. For both molecular ions, that is, HN_2^+ in Fig. 3 and HCO^+ in Fig. 6, a situation of a well-defined intersection point is approached for the case when $B^{\rm est} = B_0^{\rm exp} + \Delta B_0$. The model based on the spectroscopic correction S_0 leads to less consistent structural parameters, as verified by Table 6 for HN_2^+. The residual contributions C_0 of the zero-point motion in $B^{\rm est} = B_0^{\rm exp} + S_0$ are more pronounced for the deuterium containing forms of both HN_2^+ in Fig. 3 (middle) and HCO^+ in Fig. 6 (top). We also found that a combined analysis of all data using a nonlinear least squares procedure provides a more balanced solution and thus more accurate structural parameters than pairwise approaches (like Kraichman's equations). This conclusion fully corroborates our previous recommendation [2].

In experimental studies, the spectroscopic correction S_0 is obtained from the effective rotational constants for the ground vibrational state and singly excited vibrational ν_1, ν_2, and ν_3 states, as seen by Eq. (4). Experimental data for the fundamental vibrations are not always available also for (many) different isotopic forms. To access information relevant for the higher-order vibration-rotation contribution term C_0 by experimental means, measure-

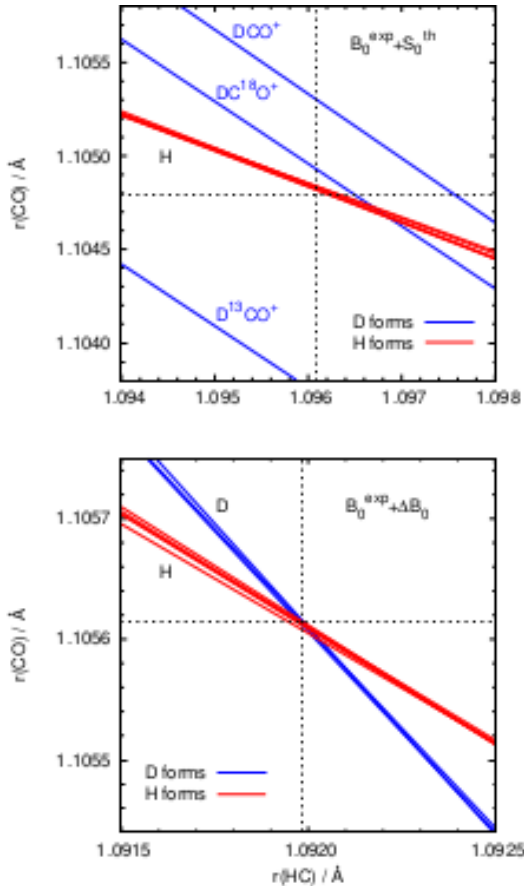

Figure 6: Pairs of the bond distances r(HC) and r(CO) that reproduce $B_e^{\rm est}$ modeled as $B_0^{\rm exp} + S_0^{\rm th}$ (top) and $B_0^{\rm exp} + \Delta B_0^{\rm th}$ (bottom) for eight isotopologues of HCO^+.

ments on vibrational overtones and combination bands are additionally required. But, this is not an easy task due to the increasing number of perturbations of the rovibrational structures which have to be identified and accounted for.

In electronic-structure program packages, the spectroscopic correction S_0 obtained by second-order vibrational perturbation theory [26] has become a standard tool for the computation of the zero-point rotational constant B_0 from the calculated equilibrium rotational constant B_e. As shown in the present study for HN_2^+ and previously for HCO^+ and HOC^+ [1, 2], this correction appears to have its own fundamental deficiency due to the neglect of higher-order effects. Electronic-structure (single-point) computations are also employed to obtain other rotational parameters but only at equilibrium, such as D_e and H_e. Their comparison with the actual experimental situation must be handled with great care, otherwise the theory may be led to improper conclusions, as demonstrated before for the case of C_3H^+ [27].

In view of the preceding analysis, full-dimensional rovibrational calculations reemerge naturally as helpful. To gather the maximum amount of information possible in such a calculation, it is essential to have a good functional form for the potential, satisfying at least the fundamental symmetries [27]. Cyanocarbene, HCCN, for instance, is a radical with a bent equilibrium structure [$\angle(\mathrm{HCC})_e$=147°, $\angle(\mathrm{CCN})_e$=175°], whose rovibrational energy pattern is well modeled by the linear-molecule convention [28]. A quartic internal coordinate force field for HCCN, covering only a narrow (near-equilibrium) part of the configuration space, may then be a serious drawback for a proper description of the dynamical behaviour of the angular degrees of freedom

[27].

The proposed strategy for the computation of ΔB_0 stands out as the most consistent method to derive a r_e structure. It can be also applied to larger molecules, since only vibrational ground state information for a sufficient set of J values is required which is much easier to compute than a full spectrum. Such a calculation requires only a moderate region of the PES which has to be combined with an exact **rovibrational** kinetic energy operator to build a full Hamiltonian which can then be treated by any numerically convenient and accurate ground state method. The observed robustness of the computed ΔB_0 values for two different PESs suggests that the level of electronic structure treatment does not have to be extremely high. **This expectation deserves computational verification. However, the total number of isotopologues required in the reconstruction procedure for larger molecules may be fairly high.**

The equilibrium geometry and spectral behaviour are not always correlated in a simple fashion, as seen in the example of HCCN. This is also manifested when determining the molecular structure from the spectral data. A molecule is defined as linear when the potential energy minimum is at a linear geometry. This definition is applied in traditional spectroscopy under the assumption that the out-of-line motion is executed so that positive and negative excursions from the line leave the molecule on average in a linear configuration. This interpretation in essence neglects the rotational aspect in the doubly degenerate bending mode. The vibrationally averaged structure of linear molecules is bent even in the ground vibrational state [29]. In connection with this, the present work also provides a qualitative rationalization

of the so-called r_0 structure, explained in terms of a structure projected onto the principal a axis. This is shown by the example of the isoelectronic series of linear triatomic molecules HCO^+, HCN, HN_2^+, HNC, and HOC^+.

Our approach for determining the equilibrium structure of the protonated nitrogen molecule is self-consistent, and the issues under our control are detailed down to the last instance. We solve it as a well-posed mathematical problem with the help of least-squares techniques, which produce equilibrium bond lengths accurate to 10^{-5}-10^{-6} Å as the least-squares solution. The physical significance of such structural parameters should not be overinterpreted, however. The most commonly used assumption in studies like the present one is to use the Born-Oppenheimer approach in combination with atomic masses (the electron masses attached to the nuclei under the point mass assumption). It is easy to verify that the influence of one single electron mass on the rotational constant is approximately 0.5 MHz. Rotational constants known to five significant digits produce structural parameters known also to five significant digits, that is, to 10^{-5} Å, in accordance with Table 2 which shows that the uncertainty of r_e is linearly proportional to the uncertainty of B_e. In our previous study on HCO^+ and HOC^+, we found that the replacement of the atomic masses with the nuclear masses affects the structural parameters in order of 10^{-4} Å, which is an effect much larger than the accepted statistical uncertainties of 10^{-5} Å found there for r_e [2]. This is consistent with the electron to proton mass ratio of $5{\cdot}10^{-4}$. We also note that the equilibrium structure obtained for HCO^+ and HOC^+ using atomic masses is found to be statistically somewhat better than the nuclear-mass results [2]. Highly consistent methods for the derivation of r_e structures are a

mandatory step on the way to identify effects beyond the Born-Oppenheimer picture and our method appears to be valuable for this enterprise.

To bring experiment/experimental observations and theory even closer, challenges ahead are associated with the manifestation of non-Born-Oppenheimer effects in real molecules, which always resolve their own eigenvalue problem exactly. In rotational spectra, this will bring in a small unknown mass-dependent contribution ΔB_e to the experimentally observed B_0, whose dominant part is the Born-Oppenheimer B_e value. This implies further that the true equilibrium parameters will be isotopologue dependent and distributed about the equilibrium Born-Oppenheiimer structure, assuming that non-Born-Oppenheimer effects are such that the notion of the potential energy surface will be sustained and the true equilibrium structure will be defined by its minimum. For diatomic molecules, there are models to incorporate the mass-dependent nonadiabatic effects into *ab initio* potential energy curves by morphing them separately for each of the isotopologues, like, for instance, Ref. [30]. Further conceptual developments are, however, required to address this issue for the case of triatomic molecules from the theoretical and experimental viewpoints in order to properly include translational and rotational invariances of entire molecular Hamiltonians.

References

[1] M. Mladenović, Theoretical spectroscopic parameters for isotopic variants of HCO^+ and HOC^+, J. Chem. Phys. 147 (2017) 114111. https://doi.org/10.1063/1.4998467.

[2] M. Mladenović, M. Lewerenz, Comparison of spectroscopic strategies to determine molecular geometries and the impact of nuclear versus atomic masses: the example of HCO^+ and HOC^+, Mol. Phys. 116 (2018) 3607–3620. https://doi.org/10.1080/00268976.2018.1464227.

[3] S. Schmatz, M. Mladenovic, Intramolecular dynamics and density of states for HN_2^+, Ber. Bunsenges. Phys. Chemie 101 (1997) 372–386. https://doi.org/10.1002/bbpc.19971010309.

[4] S. Schmatz, Globale Potentialhyperflächen und genaue Schwingungszustandsdichten am Beispiel der Kationen HN_2^+ und HCO^+, Ph.D. thesis, Georg-August-Universität Göttingen (1997).

[5] M. Mladenović, E. Roueff, Ion-molecule reactions involving HCO^+ and N_2H^+: Isotopologue equilibria from new theoretical calculations and consequences for interstellar isotope fractionation, Astron. Astrophys. 566 (2014) A144. https://doi.org/10.1051/0004-6361/201423733.

[6] X. Huang, E. F. Valeev, T. J. Lee, Comparison of one-particle basis set extrapolation to explicitly correlated methods for the calculation of accurate quartic force fields, vibrational frequencies, and spectroscopic constants: Application to H_2O, N_2H^+, NO_2^+, and C_2H_2, J. Chem. Phys. 133 (2010) 244108. https://doi.org/10.1063/1.3506341.

[7] C. E. Dateo, T. J. Lee, D. W. Schwenke, An accurate quartic force field and vibrational frequencies for HNO and DNO, J. Chem. Phys. 101 (1994) 5853–5859. https://doi.org/10.1063/1.467301.

[8] M. Mladenović, Z. Bačić, Highly excited vibration-rotation states of floppy triatomic molecules by a localized representation method: The HCN/HNC molecule, J. Chem. Phys. 93 (1990) 3039–3053. http://dx.doi.org/10.1063/1.458838.

[9] M. Mladenović, S. Schmatz, Theoretical study of the rovibrational energy spectrum and the numbers and densities of bound vibrational states for the system HCO^+/HOC^+, J. Chem. Phys. 109 (1998) 4456–4470. http://dx.doi.org/10.1063/1.477049.

[10] W. H. Press, B. P. Flannery, S. A. Teukolsky, W. T. Vetterling, Numerical Recipes, Cambridge University Press, Cambridge, 1986.

[11] S. Yu, J. Pearson, B. Drouin, T. Crawford, A. Daly, B. Elliott, T. Amano, Rotational spectroscopy of vibrationally excited N_2H^+ and N_2D^+ up to 2.7 THz, J. Mol. Spectrosc. 314 (2015) 19–25. https://doi.org/10.1016/j.jms.2015.05.001.

[12] J. C. Owrutsky, C. S. Gudeman, C. C. Martner, L. M. Tack, N. H. Rosenbaum, R. J. Saykally, Determination of the equilibrium structure of protonated nitrogen by high resolution infrared laser spectroscopy, J. Chem. Phys. 84 (1986) 605–617. https://doi.org/10.1063/1.450607.

[13] T. Amano, T. Hirao, J. Takano, Submillimeter-wave spectroscopy of

HN_2^+ and DN_2^+ in the excited vibrational states, J. Mol. Spectrosc. 234 (2005) 170–175. https://doi.org/10.1016/j.jms.2005.09.004.

[14] G. Cazzoli, L. Cludi, G. Buffa, C. Puzzarini, Precize THz measurements of HCO^+, N_2H^+, and CF^+ for astrophysical observations, Astrophys. J. Suppl. Ser. 203 (2012) 11. https://doi.org/10.1088/0067-0049/203/1/11.

[15] L. Dore, L. Bizzocchi, E. S. Wirström, C. Degli Esposti, F. Tamassia, S. B. Charnley, Doubly ^{15}N-substituted diazenylium: THz laboratory spectra and fractionation models, Astron. Astrophys. 604 (2017) A26. https://doi.org/10.1051/0004-6361/201629725.

[16] J. Koput, Ab initio structure and vibration-rotation dynamics of the formyl and isoformyl cations, HCO^+/HOC^+, J. Chem. Phys. 150 (2019) 154307. https://doi.org/10.1063/1.5089718.

[17] J. Kraitchman, Determination of molecular structure from microwave spectroscopic data, Amer. J. Phys. 21 (1953) 17–24. https://doi.org/10.1119/1.1933338.

[18] C. C. Costain, Determination of molecular structures from ground state rotational constants, J. Chem. Phys. 29 (1958) 864–874. https://doi.org/10.1063/1.1744602.

[19] P. G. Szanto, T. G. Anderson, R. J. Saykally, N. D. Piltch, T. A. Dixon, R. C. Woods, A microwave substitution structure for protonated nitrogen N_2H^+, J. Chem. Phys. 75 (1981) 4261–4263. https://doi.org/10.1063/1.442628.

[20] H. E. Warner, The microwave spectroscopy of ions and other transient species in dc glow and extended negative glow discharges, Ph.D. thesis, University of Wisconsin-Madison (1988).

[21] M. Mladenović, Rovibrational hamiltonians for general polyatomic molecules in spherical polar parametrization. I. Orthogonal representations, J. Chem. Phys. 112 (2000) 1070–1081. https://doi.org/10.1063/1.480662.

[22] M. Mladenovic, unpublished.

[23] E. F. Pearson, R. A. Creswell, M. Winnewisser, G. Winnewisser, The molecular structures of HNC and HCN derived from the eight stable isotopic species, Z. Naturforsch. A 31 (1976) 1394–1397. https://doi.org/doi:10.1515/zna-1976-1119.

[24] J. K. G. Watson, The estimation of equilibrium molecular structures from zero-point rotational constants, J. Mol. Spectrosc. 48 (1973) 479–502. https://doi.org/10.1016/0022-2852(73)90112-4.

[25] V. Špirko, O. Bludský, W. P. Kraemer, Energies and electric dipole moments of the bound vibrational states of HN_2^+ and DN_2^+, Collect. Czech. Chem. Commun. 73 (2008) 873-897. http://doi:10.1135/cccc20080873.

[26] C. Puzzarini, J. F. Stanton, J. Gauss, Quantum-chemical calculation of spectroscopic parameters for rotational spectroscopy, Int. Rev. Phys. Chem. 29 (2010) 273–367. https://doi.org/10.1080/01442351003643401.

[27] M. Mladenović, The B11244 story: Rovibrational calculations for

C_3H^+ and C_3H^- revisited, J. Chem. Phys. 141 (2014) 224304. https://doi.org/10.1063/1.4903251.

[28] M. Mladenović, P. Botschwina, C. Puzzarini, Six-dimensional potential energy surface and rovibrational energies of the HCCN radical in the ground electronic state, J. Phys. Chem. A 110 (2006) 5520–5529. https://doi.org/10.1021/jp056743u.

[29] G. Winterhoff, S. Galleguillos Kempf, P. Jensen, P. Bunker, Empirical potential energy surface and bending angle probability densities for the electronic ground state of HCO^+, J. Mol. Spectrosc. 354 (2018) 71–82. https://doi.org/10.1016/j.jms.2018.10.004.

[30] L. D. Augustovičová, V. Špirko, Radial molecular property functions of CH in its ground electronic state, J. Quant. Spectrosc. Radiat. Transf. 272 (2021) 107809. https://doi.org/10.1016/j.jqsrt.2021.107809.

Graphical Abstract

Accurate equilibrium structures of linear triatomic molecules from a combined theoretical-experimental method: The protonated nitrogen molecule, HN_2^+

Mirjana Mladenović, Marius Lewerenz

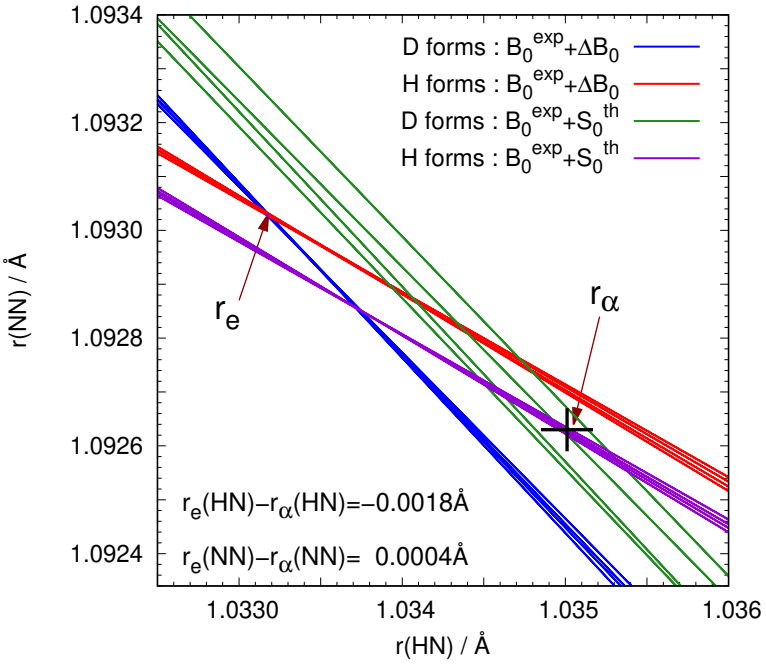

Highlights

Accurate equilibrium structures of linear triatomic molecules from a combined theoretical-experimental method: The protonated nitrogen molecule, HN_2^+

Mirjana Mladenović, Marius Lewerenz

- Strategies to derive molecular equilibrium structures from experimental data.
- α constants are insufficient to obtain accurate r_e structures from B_0.
- Rovibrational variational calculations for HN_2^+ for two potential energy surfaces.
- Theoretical zero-point corrections are insensitive to *ab initio* level.